UNIVERSITYOF BIRMINGHAM

Behaviour of traffic emitted semi-volatile and intermediate volatility organic compounds within the urban atmosphere

Xu, Ruixin; Alam, Mohammed S.; Stark, Christopher; Harrison, Roy M.

[Link to publication on Research at Birmingham portal](#)

Journal Pre-proof

Behaviour of traffic emitted semi-volatile and intermediate volatility organic compounds within the urban atmosphere

Ruixin Xu, Mohammed S. Alam, Christopher Stark, Roy M. Harrison

Please cite this article as: R. Xu, M.S. Alam, C. Stark, et al., Behaviour of traffic emitted semi-volatile and intermediate volatility organic compounds within the urban atmosphere, *Science of the Total Environment* (2018), https://doi.org/10.1016/j.scitotenv.2020.137470

Behaviour of Traffic Emitted Semi-Volatile and Intermediate Volatility Organic Compounds Within the Urban Atmosphere

Ruixin Xu, Mohammed S. Alam, Christopher Stark and Roy M. Harrison[*†]

Division of Environmental Health and Risk Management, School of Geography, Earth and Environmental Sciences University of Birmingham Edgbaston, Birmingham B15 2TT United Kingdom

---

[*] To whom correspondence should be addressed.
Tele: +44 121 414 3494; Fax: +44 121 414 3709; Email: r.m.harrison@bham.ac.uk

[†]Also at: Department of Environmental Sciences / Center of Excellence in Environmental Studies, King Abdulaziz University, PO Box 80203, Jeddah, 21589, Saudi Arabia
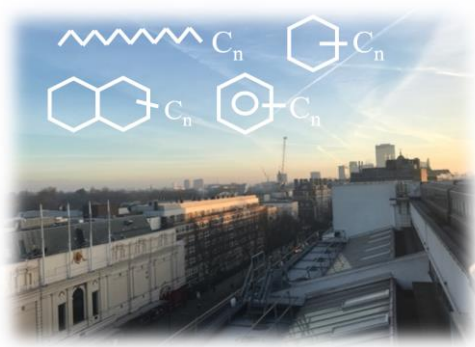
Graphical abstract

Caption: A view from the roof sampling site WM overlooking Marylebone Road (MR).

ABSTRACT

Particulate matter originated from traffic has attracted major interest over the last few years. The semi-volatile organic component of the particles may evaporate with dispersion away from the emission source, creating vapour which may oxidise to form secondary organic aerosol. Air samples were collected from a street canyon, the adjacent park and an urban background site during the winter-spring period in central London, UK. Emissions of semi-volatile organic compounds (SVOCs) and intermediate volatility organic compounds (IVOCs) ranging from C_{10} to C_{36} in both the gas phase and particle phase were measured by using thermal desorption coupled to comprehensive two-dimensional gas chromatography time-of-flight mass spectrometry (TD-GC×GC-ToF-MS). Main compound groups identified and quantified were grouped alkanes (n-alkanes and branched alkanes), monocyclic alkanes, bicyclic alkanes and monocyclic aromatics. The carbon preference index (CPI) of n-alkanes was estimated to distinguish the emission sources. Pearson correlations between I/SVOCs and traffic tracers (black carbon, NO_x and benzene) in different locations were compared to analyse the influence of this emission source. The results indicate that while the major emission source at the roadside site is traffic, the lower correlations at background sites are indicative of other source contributions and/or differential reactivity of compounds. Gas-particle phase partitioning of n-alkanes is evaluated and compared between sites. The potential influence of gas phase I/SVOCs upon OH reactivity and secondary organic aerosol formation is estimated and found to be relatively small.

3

1. INTRODUCTION

Roadside particles are a complex mixture of pollutants from multiple origins, including both anthropogenic and biogenic sources. As a major emission source within the urban environment, particulate matter originated from traffic has attracted major interest over the last few years. At a London roadside site, 72% of particles by number arose from traffic on the adjacent roadway (Harrison et al., 2011), and a large component of the traffic particles has the potential to evaporate (Harrison et al., 2016). A substantial fraction of traffic emitted primary particles has been shown to be semi-volatile (Robinson et al., 2007; May et al., 2013) and mainly comprised of aliphatic species with carbon number from C_{12} to C_{35} (Alam et al., 2018; 2016a). Intermediate volatility organic compounds (IVOCs) refer to species with an effective saturation concentration C^* between 10^4 and 10^7 μg m^{-3} while semi-volatile organic compounds (SVOCs) refer to organic species with C^* between 1 and 10^3 μg m^{-3} (Robinson et al, 2007). Typically, IVOCs range from C_{13} to C_{22} while SVOCs range from C_{22} to C_{30}. Most previous research studies on atmospheric samples processed by GCMS have focused on a limited range of tracer compounds and homologous series that can be distinguished from the bulk of mass, typically involving n-alkanes, PAHs, hopanes and steranes (Lewis et al., 2000; Kawashima et al., 2006; Omar et al., 2007; He et al., 2008). These species only account for a small portion of the total mass or number of compounds in the exhaust. The remaining semi-volatile emissions can play an important role in photochemical smog formation and are likely to become a source of SOA (Alam et al., 2018; Schauer et al., 1999). In addition, relatively few studies conducted on the atmospheric abundance of gaseous hydrocarbons above C_{12} (Fraser et al., 1997; Zhao et al., 2014; Chan et al., 2013; Lyu et al., 2019) although the diesel vehicle-emitted organic compounds consist largely of higher molecular weight species up to C_{30} (Alam et al., 2018; Schauer et al., 1999; Lu et al., 2018; Cross et al., 2015; Worton et al., 2014). Xu et al. (2019) reported measurements of I/SVOC compound groups in air samples by GC×GC-TOF-MS collected from a ground-level roadside site, an adjacent rooftop site, a nearby park and an urban background site in London, UK, as a part of the FASTER campaign. The organic groups identified

include C_{13}-C_{36} acyclic alkanes (branched and linear alkanes), C_{12}-C_{25} monocyclic alkanes (i.e. alkyl-cyclopentane, alkyl-cyclohexane, alkyl-cycloheptane and their derivatives), C_{13}-C_{27} bicyclic alkanes (i.e. alkyl-decalin and derivatives) and C_{10}-C_{24} monocyclic aromatics. However, a number of research questions remain unanswered, concerning the behaviour of these I/SVOCs in the atmosphere.

Intermediate volatility and semi-volatile organic compounds (I/SVOCs) are compounds that can partition between the gas phase and particle phase in the atmosphere. As the particles disperse away from the emission source, the semi-volatile organic component of the particles may evaporate releasing vapour due to a difference between the ambient and equilibrium vapour pressures (Robinson et al., 2007). The partitioning of I/SVOCs is an important process that affects many issues, such as the formation of secondary organic particles and the role of organic aerosols in climate change (Arp et al., 2008). Gas/particle (G/P) partitioning varies with changing atmospheric conditions. Generally, it reaches an equilibrium depending upon the temperature, and for some compounds relative humidity of the environment, the concentration and composition of particulate matter, and vapour pressure of the compound (Yamasaki et al., 1982; Pankow and Bidleman, 1992). G/P partitioning also affects a compound's atmospheric fate, its lifetime in the air, its deposition, and its transformation and transport (Pankow and Bidleman, 1992; Bidleman et al., 1986; Mader and Pankow, 2001; Sangiorgi et al., 2014).

Laboratory experiments have demonstrated that the photo-oxidation of low-volatility gas-phase species rapidly generates significant secondary organic aerosol (SOA) (Weitkamp et al., 2007; Leskinen et al., 2007). The oxidation process in the gas phase may add functional groups to the precursor molecule, producing lower-volatility compounds that condense into the particle phase (Jathar et al., 2012). Pye and Seinfeld (2010) estimated the global production of organic aerosol from primary emission of I/SVOCs, predicting that I/SVOC oxidation is a larger source of net

aerosol production than oxidation of traditional parent hydrocarbons (terpenes, isoprene and aromatics). Past studies have typically classified the alkane homologues by volatility based on the retention times due to the challenges in speciating alkane isomers (Grieshop et al., 2009; Presto et al., 2012; Dunmore et al., 2015). Lack of understanding on the molecular structure can cause uncertainties in the study of the SOA formation from these hydrocarbons, as SOA yields change with the alkane structure (linear, branched and cyclic) and number of rings (Pye and Pouliot, 2012; Loza et al., 2014; Lim and Ziemann, 2009; Tkacik et al., 2012). Therefore, information on the molecular structure is crucial to understanding the environmental fate of these semi-volatile compounds.

This study applied molecular diagnostic parameters for n-alkanes and a correlation analysis between I/SVOCs and traffic indicators to distinguish the emission sources of the I/SVOCs identified in the FASTER London Campaign 2017. The partitioning of n-alkanes between the gas phase and the particle phase is analysed, and primary OH reactivity and potential for SOA formation are also considered.

2. EXPERIMENTAL

2.1 Field Measurements

Multiple-site measurements were conducted in central London (UK) as a part of the FASTER campaign (Harrison et al., 2019) to quantify the changes in the composition of I/SVOCs during the advection (horizontal transport) from the traffic to the cleaner atmosphere of a downwind park. The four sampling sites include a kerbside cabin (inlet around 2.5 metres above ground level) on the south sidewalk of the heavily trafficked Marylebone Road (MR) where the traffic flow is over 80,000 vehicles per day from 22 March to 18th April 2017; a roof (around 26 metres high) of the University of Westminster (WM) at the south side of the Marylebone Road overlooking the MR sampling site between 24 January 2017 and 19 February 2017; a roof (around 16 metres high) of

6

Regent's University (RU) which is located to the south of the Inner Circle of Regent's Park and about 380 m north of heavily trafficked Marylebone Road at the same time as WM sampling; and an urban background site Eltham (EL) in the southeast of London from 23 February to 21 March 2017 (Figure S1 and Table S1). During the London field campaign 2017, an in-house auto-sampler collected 24h duration ambient air samples continually for seven days. The sampler has seven channels and is turned to the next channel automatically after 24h. A flow rate meter is set in to manage the flowrate which was set as 1.5L min^{-1} during the sampling. Ambient air was drawn by a vacuum pump through a polypropylene backed PTFE filter (47 mm, 1 μm pore, Whatman, Maidstone, UK) to collect the particulate phase and subsequently through a stainless-steel thermal adsorption tube packed with 1 cm quartz wool, 300 mg Carbograph 2TD 40/60 (Markes International) to collect the gas phase (Xu et al. 2019). After collection, filters and tubes were stored at below −18℃ before the extraction and GC×GC-ToF-MS analysis.

2.2 Analysis by GC×GC-ToF-MS

Analyses were conducted using an Agilent 7890B gas chromatograph (Agilent Technologies, Wilmington, DE, U.S.A.) equipped with a Zoex ZX2 cryogenic modulator (Houston, TX, U.S.A.). Adsorption tubes were desorbed using thermal desorption (Unity 2, Markes International, Llantrisant, UK).Particulate phase samples were extracted with dichloromethane (HPLC grade) prior to analysis, using ultrasonic agitation for 20 mins at room temperature before concentrating to a volume of approximately 50 μl by a stream of dry nitrogen gas (Xu et al, 2019). A nonpolar capillary SGE BPX5 column (30 m, 0.25 mm ID, 0.25 μm-5% phenyl polysilphenylene-siloxane) was equipped for the first-dimension of GC×GC to separate the compounds based on their volatility while a SGE BPX50 (4 m, 0.1 mm ID, 0.1 μm-50% phenyl polysilphenylene-siloxane) column was equipped for the second-dimension to separate the compounds based on their polarity. The two-dimensional gas chromatograph was coupled with a BenchToF-Select-time-of-flight mass spectrometer (Markes International, Llantrisant, UK) operated with traditional electron impact

ionisation at 70 eV to provide masses of the ionised molecule and its fragments. The scan speed was 50 Hz with a mass resolution of >1200 full width at half maximum (fwhm). The GC sensitivity derived from the injection of 1pg octafluoronaphthalene (m/z =272), showing an S/N (signal to noise) ratio of >2000:1 rms (Alam et al., 2016b). Detection limits are listed in the Supplementary Information. A modulation time of 11s was applied while a total run time for each sample was 120min. Subsequent data processing was conducted using GC Image_ v2.6 (Zoex Corporation). Samples were spiked with 9 deuterated internal standards for qualification, including dodecane-d26, pentadecane-d32, eicosane-d42, pentacosane-d52, triacontane-d62, biphenyl-d10, n-butylbenzene-d14, n-nonylbenzene-2, 3, 4, 5, 6-d5 (Chiron AS, Norway) and p-terphenyl-d14 (Sigma Aldrich, UK). More details of the instrument settings and sample analysis methods are given in our previous papers (Alam et al., 2016a; Xu et al., 2019; Alam et al., 2016b).

GC×GC-ToF-MS allows compounds with similar physicochemical properties to be classified as chemical classes based on their retention behaviour. This research assigned individual compounds to particular chemical classes and grouped the chemical compounds into isomer sets based on their carbon number and functional group. For example, individual n-alkanes ranging from the C_{13}-C_{31} in the gas phase and C_{13}-C_{36} in the particle phase were identified and quantified. The alkane isomer sets were mapped on the chromatogram based on their retention behaviour in GC×GC and quantified by adapting linear n-alkanes with same carbon number as surrogates to estimate the concentrations of total alkanes including linear alkanes and branched alkanes. For calibration and quantification of the isomer groups, 72 natural standards were applied to cover as much of the chromatogram as possible. Natural standards include n-alkanes (C_{11}-C_{36}), phytane and pristane (Sigma Aldrich, UK), n-alkyl-cyclohexanes (C_{11} -C_{25}), n-alkylbenzenes (C_{10}, C_{12}, C_{14}, C_{16} and C_{18}), tetralin, alkyl-tetralins (methyl-, di-, tri- and tetra-), cis- and trans-decalin, alkyl-naphthalenes (C_{11}, C_{12}, C_{13} and C_{16}) (Chiron AS, Norway) and 13 polycyclic aromatic hydrocarbons (Thames Restek UK Ltd). The overall uncertainties of this quantification method have been calculated as 24% and

8

reported by Alam et al. (2018). More details of mapping the isomer sets are described by Xu et al. (2019) and Alam et al. (2018). The retention behaviour allows locations of more compound classes in the chromatogram. Compound groups identified within the ambient air samples included C_{13}-C_{36} alkanes (n+i), C_{12}-C_{25} monocyclic alkanes, C_{13}-C_{27} bicyclic alkanes, C_{10}-C_{24} monocyclic aromatics, C_{11}-C_{16} naphthalenes, C_{13}-C_{15} biphenyls, C_{15}-C_{16} phenanthrenes/ anthracenes, C_{14}-C_{15} fluorenes and C_{12}-C_{13} tetralins, accounting for approximately 78% of the total ion current of the chromatogram. Alkanes (n+i) (36%-57%), monocyclic alkanes (17%-24%), bicyclic alkanes (8%-15%) and monocyclic alkanes (15%-18%) dominated the overall I/SVOC concentrations identified in the four sampling sites. Individual C_{13}-C_{36} n-alkanes and C_{12}-C_{25} n-alkyl cycloalkanes were also identified and quantified.

2.3   Supporting Measurements

Air samplers operated on behalf of the UK Department for Environment, Food and Rural Affairs (DEFRA) (https://uk-air.defra.gov.uk/networks/) offer hydrocarbon and other pollutant data at the Marylebone Road and Eltham monitoring stations used in this study. The hourly-average concentrations of n-alkanes ranging from C_2-C_8 at the Marylebone Road and Eltham sites collected by the DEFRA network were averaged into 24h durations and plotted alongside the C_{13}-C_{31} n-alkanes measured by GC×GC-ToF-MS in this study (Figure 1). Measurements of the black carbon (BC) content of airborne particles were carried out at the roof sites WM and RU by using a 2 Wavelength Magee Aethalometer AE22 (ultraviolet 370 nm for UV components and infra-red 880 nm for BC) with sensitivity of around 0.03 μg/m^3 @ 1 min, 5 LPM.

BC, NO$_x$ and benzene concentrations at MR and EL were measured by the DEFRA network. The correlation between I/SVOCs and traffic indicators (BC, NO$_x$ and benzene) were calculated to assess the contribution of traffic to concentrations at Marylebone Road and Eltham. Temperature and wind information during the London Campaign 2017 was taken from Heathrow Airport located

in the west of London (Met Office, 2006) The temperature at Heathrow is slighter lower than central London (average 1-2℃) due to the influence of the urban heat island. The percentage differences in temperature are very small and hence insignificant as the temperature is eventually expressed in Kelvin in the gas-particle partitioning calculations.

3.   RESULT AND DISCUSSION

3.1   Homologue Distribution and Diagnostic Ratios of n-Alkanes

Individual n-alkanes were separated and identified in this research, showing the average concentrations of n-alkanes from C_{13} to C_{31} in the gas phase and C_{13} to C_{36} in the particle phase at the four sampling sites (Table 1). The total concentrations of n-alkanes in the particle phase were lower than the gas phase, with the more volatile n-alkanes (C_{13}-C_{18}) were the most abundant homologues in the gas phase, while the less volatile n-alkanes (C_{20} to C_{30}) were more abundant in the particle phase. Xu et al. (2019) presented the concentrations and variabilities of main I/SVOC groups at each site, including acyclic alkanes (n+i), monocyclic alkanes, bicyclic alkanes and monocyclic aromatics. The concentrations of individual n-alkanes correlated well with grouped acyclic alkanes ($0.5<$ average $R^2 <0.8$). The correlation coefficients between n-alkanes and grouped alkanes (n+i) significantly decreased after C_{25} in the gas phase and after C_{31} in the particle phase, indicating a change in the composition of high molecular weight alkanes (n+i). For those high molecular weight alkanes (n+i), there are decreased contributions from linear n-alkanes accompanied by an increased contribution from branched i-alkanes. The number of possible isomers increases with the increase of the number of carbon atoms (Goldstein and Galbally, 2007), resulting in a greater contribution of branched alkanes to the high molecular weight alkanes (n+i). Total n-alkanes occupied on average 33% of the total alkanes (n+i), and the branched alkanes accounted for the rest. Chan et al. (2013) identified linear and branched alkanes ranging from C_{20} to C_{25} emitted from fossil fuel-related sources. The relative ratios of total branched alkanes to linear

10

alkanes reported by Chan et al. (2013) vary greatly from ~1 to >10 between urban sampling sites, which is in broad agreement with this study (Ratio=2).

The carbon distribution of the hydrocarbon classes at the roadside site were very similar to that in the urban background sites (R^2=0.62-0.88), consistent with n-alkanes (R^2=0.64-0.96). The average mass concentrations were higher at the road site MR in comparison to the two roof sites WM and RU, and the concentrations at WM were slightly higher than RU. The concentrations of I/SVOCs were reduced with the larger distance of the sampling sites from the main traffic sources.

The DEFRA measurements offer n-alkanes ranging from C_2-C_8 at MR and EL. Figure 1 shows the consistency between DEFRA network n-alkanes (C_2-C_8) and GC×GC-MS measured n-alkanes in the gas phase (C_{13}-C_{30}). With the increase of the carbon number, the concentrations of n-alkanes in the gas phase had a downward trend as emissions decline and the low-volatility homologues partition to the particle phase. A summary of the n-alkane concentrations reported in the literature is shown in Table 2. The magnitude of n-alkane concentrations measured in this study was similar to that for n-alkanes reported by Cincinelli et al. (2007), Gupta et al. (2017), Nikolova et al. (2016) and Mandalakis et al. (2002) but much lower than those reported by Bi et al. (2003) and Karanasiou et al. (2007). The carbon distribution of n-alkanes shown in Table 1 shows a strong similarity to that for n-alkanes measured in Delhi, India (Gupta et al., 2017) and Birmingham, UK (Nikolova et al., 2016) but differs from the gas-phase n-alkane measured in Prato Italy (Cincinelli et al., 2007) and Athens Greece (Mandalakis et al., 2002), probably due to the different fuel use and road conditions.

Diagnostic ratios have been widely used in previous studies as the homologue distribution is strongly related to the formation mechanism of organic aerosols (Simoneit et al., 2004; Andreou and Rapsomanikis, 2009). Carbon preference index (CPI) is the ratio of the summation of odd carbon number homologues to the summation of even carbon number homologues over the same

range of carbon numbers (Cincinelli et al., 2007; Andreou and Rapsomanikis, 2009; Simoneit, 1999). CPI provides a suitable molecular-based marker for tracing the organic input of vegetation, as plant waxes emit higher molecular weight n-alkanes with odd carbon number predominance (Simoneit, 1999). The leaf wax is expected to contribute less to the overall emissions of n-alkanes during this winter-early spring sampling period compared with summer as many local trees are deciduous. CPI values for traffic emissions and other anthropogenic activities are close or lower than 1. CPI values typically range from 1 to 2 for urban environments with dominant traffic emission sources while higher CPI values above 2 are observed for rural areas where the biogenic influence is more significant (Alves, 2008; Mirante et al., 2013).

The average CPI values were calculated for both the gas and particle phase at each sampling site (Table 1). The carbon number of the most abundant alkane (C_{max}) can also be used as an indicator of the input source (Mazurek and Simoneit, 1984; Omar et al., 2007). CPI values varied little between the sampling sites in central London (WM, RU and MR). In the gas phase, n-alkanes from C_{13} to C_{31} were detected at all sampling sites with a C_{max} at C_{13}. Average CPI values at WM, RU and MR were close to unity (1.07, 1.13 and 1.05 respectively), associating a fossil fuel source, likely to be vehicle emissions, with the gas phase n-alkanes. Gas phase n-alkanes at the urban background site (EL) had a higher odd carbon number predominance (higher CPI value 1.44), indicative of a greater contribution of n-alkanes originated from plant wax. In the particle phase, n-alkanes from C_{13} to C_{36} were detected and C_{max} values varied from C_{20} to C_{22} at the four sampling sites. CPI values measured for n-alkanes at all four sampling sites were close to 1, signifying fossil fuels as the dominant emission source. The plant wax-derived n-alkanes are typically heavier n-alkanes (above C_{27}) with a strong odd carbon number predominance (Andreou and Rapsomanikis, 2009). The CPI values (above C_{25}) are higher than the CPI (C_{13}-C_{26}), especially at WM, RU and MR, suggesting that plant wax made a larger contribution to the heavier alkanes, as is expected.

3.2   Correlations with Traffic Emissions

Concentrations of grouped chemicals and individual chemical compounds appear in Table S2-S3. Black carbon (BC) and NO_x are regarded as indicators for diesel-powered vehicles, as a substantial proportion of BC and NO_x come from diesel vehicles in London (Harrison and Beddows, 2017). Benzene was used to trace the association between the gasoline vehicles and I/SVOCs as these are the major urban source of the compound (NAEI, 2019). Correlations were carried out between the I/SVOCs (sum of gas and particle phase) with the traffic indicators, and the correlation coefficient R as a function of the carbon number is shown as Figure 2.

As expected, I/SVOC concentrations showed the highest correlation with NO_x and BC at the roadside MR site, indicating that the majority of I/SVOC emissions at MR were attributed to traffic. MR is a street canyon site where the buildings prevent the rapid dilution of I/SVOCs emitted from traffic by exchanging with the incoming air, and traffic emissions can be considered as a dominant source (Wehner et al., 2002). The alkane classes (acyclic and cyclic) correlated well with NO_x and BC, as they are the most abundant observed mass fraction in diesel fuel and lubricating oil (Isaacman et al., 2012; Worton et al., 2014; Sakurai et al., 2003; Alam et al., 2018). Acyclic alkanes (n+i), cyclic alkanes and monocyclic aromatics ranging C_{12} to C_{26} correlated steadily with traffic indicators BC or NO_x with correlation coefficient R up to 0.7, suggesting that BC or NO_x explained around 50% of the variance in the I/SVOC concentrations at MR. The correlation coefficient R of alkanes (n+i) had a slight decrease above C_{26}, suggesting the presence of other emission sources for high molecular weight alkanes (n+i) at MR, as suggested by the CPI results in Table 1. Charron et al. (2019) also reported that n-alkanes between C_{19} and C_{26} collected from a near-traffic site had a significant correlation with traffic indicator NO_x and elemental carbon (EC). The n-alkanes emitted from traffic comprise the C_{10}-C_{34} homologues, but n-alkanes ranging from C_{18} to C_{25} are predominant homologues and correspond to the high boiling point components of diesel fuel (Alves et al., 2016). At the WM and RU sites, correlations are less strong and are high only from C_{10} to

13

around C_{18}, indicating the presence of other emission sources for the background sites (e.g. biogenic source). The diesel vehicle-related I/SVOC concentrations at WM and RU dropped at around C_{18} and tended to be negligible after C_{20}, probably due to the better measurement precision for the lower molecular weight I/SVOC, or possibly due to the traffic source contributing more significantly for $< C_{18}$ compounds as emission profiles indicate there are substantial emissions of $<C_{18}$ from vehicles (Lu et al., 2018).

The correlations with benzene are shown for MR only in Figure 2 and show that these are high (up to R = 0.8) in the range C_{11} to C_{18}. The much lower correlation for alkanes of $> C_{18}$ for benzene than for BC or NO_x at this site suggests diesel emissions appear to drive variation for this molecular weight range over gasoline emissions. The gasoline emitted IVOCs mainly have volatility similar to C_{12}-C_{14} n-alkanes and include aliphatic species, aromatics and unspeciated UCM (Drozd et al., 2019; Zhao et al., 2016).The similarities in I/SVOC profiles in the ambient air of London and diesel exhaust (average R=0.84) further illustrate the impact of diesel-powered vehicles to the urban air quality (Xu et al., 2019). Besides traffic exhaust, other emission sources may also contribute to the I/SVOCs detected in current study, such as tyre and brake lining wear (Rogge et al., 1993; Pant and Harrison, 2013; Kwon and Castaldi., 2012; El Haddad et al., 2009), the use of volatile chemical products (VCPs) (McDonald et al., 2018) and asphalt-related road paving and repair (Khare and Gentner, 2018).

3.3   Analysis of n-Alkane Gas-Particle Partitioning

A critical consideration in understanding and modeling the atmospheric transport and removal of semi-volatile organic components is the distribution of these substances between the gas (or vapour) and particle phases (G/P) (Foreman and Bidleman, 1990). The distribution of a semi-volatile compound between the gas phase and particulate phase in the atmosphere is defined by using partition coefficient Kp (Pankow and Bidleman, 1992; Pankow, 1994):

Kp= (F/TSP)/A

where F and A are the chemical concentrations (ng/m^3) in the particulate phase and the gas phase respectively, and TSP is the total suspended particulate (μg/m^3). TSP was estimated based on the concentrations of PM$_{10}$ divided by 0.8 for the urban traffic (Filliger et al., 1999). PM$_{10}$ data were taken from the DEFRA North Kensington national network monitoring site.

Partitioning to the particulate matter increases with the increase of Kp (Pankow and Bidleman, 1992). For a given sample of particulate matter at a given temperature, Kp tends to be correlated with the sub-cooled liquid vapor pressure (VPt, torr) according to the following equation (Pankow, 1994):

LogKp=m$_r$log(VPt)+b$_r$

The vapour pressure values were calculated for the mean daily temperature by UManSysProp v1.0 (UmanSysProp, 2016), which is an online tool to estimate the vapour pressure of organic compounds at a given temperature by selecting from a list of methods, as explained by Topping et al. (2016), and reviewed by Barley and McFiggans (2010) and O'Meara et al. (2014). This study selected the vapour pressure method provided by Compernolle et al. (2011) as the vapour pressure of n-alkanes derived from this method is closest to the lab results from our group (Alam et al., 2019). Theory predicts that the slope value m$_r$ should be near -1 under equilibrium conditions for either adsorptive or absorptive partitioning and there is some compound to compound similarity in b$_r$ (Pankow and Bidleman, 1992; Pankow, 1994).

The values of log Kp were regressed upon log (VPt) for all n-alkanes (C$_{13}$ to C$_{29}$) for all samples at MR and RU are presented in Figure 3 while the slopes (m$_r$) and intercept (b$_r$) on each day in the

15

London Campaign 2017 appear in Table S4-S7. The slopes of these regressions on each day ranged from -0.13 to -0.42 with an average R^2 of 0.68±0.16 for WM; ranged from -0.20 to -0.42 with an average R^2 of 0.77±0.09 for RU; ranged from -0.22 to -0.54 with an average R^2 of 0.71±0.11 for MR, and ranged from -0.10 to -0.40 with an average R^2 of 0.52±0.15 for EL. This study reported a good fit to the regression relationship between *log Kp* versus *log(VPt)* for n-alkanes, but slopes (m_r) were shallower than the theoretical value of -1 according to equilibrium conditions. The m_r values at MR were relatively closer to the theoretical value of -1 compared with other sites. A previous FASTER study (Lyu et al., 2019) reported the calculated *log Kp* versus *log(VPt)* for alkanals (C_{10}-C_{14}), alkan-2-ones(C_{10}-C_{18}) and alkan-3-ones(C_{10}-C_{16}) for each day collected at four sites in the London Campaign 2017, and showed the best fit to the regression equation was at MR. It is not easy to explain the differences among sites. One possible explanation could be that gas-particle partitioning was closer to equilibrium at MR as the increased particle surface area at MR enhanced the kinetics of gas-particle exchange (Lyu et al., 2019). The difference in ambient temperature (0.4-11.4°C during WM/RU measurements, 4.1-12.7°C during EL measurements, and 8.2-15.5°C during MR measurements) might be one of the reasons causing the differences in the slope values m, among sites.

There are notable differences in reported m_r and b_r values in the literature. Some are close to the theoretical value of -1 while significant deviations have also been reported. Many reasons have been discussed to explain the variability of slopes m_r and these deviations do not always indicate disequilibrium (Terzi and Samara, 2004). Recently, a few studies have worked on the gas-particle partitioning of n-alkanes (Cincinelli et al., 2007; Mandalakis et al., 2002; Karanasiou et al., 2007) and PAHs (Mandalakis et al., 2002; Callén et al., 2008; Fernández et al., 2002; Gaga and Ari, 2011), showing significantly shallower m_r values ranging around -0.5 (Lyu et al., 2019). Slopes shallower than -0.6 are characteristic of absorption into the organic matter, while those steeper than -1 are generally interpreted to be attributed to adsorption on particle surfaces (Callén et al., 2008;

16

Fernández et al., 2002). Other reasons associated with the shallow slopes have been discussed by

Terzi and Samara (2004) and Callén et al. (2008), such as (a) chemical reaction in the ambient air;

(b) presence of nonexchangeable I/SVOC fractions on particulate matter; (c) slow gas-to-particle

sorption of the heavier compounds with lower volatility; (d) pollution sources close to the sampling

site, so that the emitted compounds are in disequilibrium; (e) difference in energy-related terms (i.e.

activity coefficients, adsorption sites and enthalpies) that are affected by the chemical composition

of the particles. Regarding the temperature variations during the sampling, there is no clear

evidence indicating that fluctuations of temperature are responsible for shallower slopes. Steeper

slopes can be observed in a study in which temperature changes are greater than 10ºC while shallow

slopes are seen in studies with temperature fluctuations lower than 6°C (Callén et al., 2008).

The slopes observed in London are broadly similar to other studies of n-alkanes. The reason for the

shallow slopes is uncertain, but given the proximity of our sites to traffic sources, disequilibrium is

a major possibility.

3.4   Estimates of Potential Secondary Organic Aerosol Formation

Recent studies have proposed that low-volatility organic vapour can lead to the significant

production of secondary organic aerosols (SOA), but these gas phase organics are not included in

many model studies (Robinson et al., 2007; Presto et al., 2010; Lim and Ziemann, 2005; 2009). The

larger hydrocarbons (above C_{12}) identified in this research represent a substantial part of what is

referred to as unspeciated chemicals in other studies, so the contribution of different traffic emitted

I/SVOC groups to the potential SOA formation can be more accurately estimated using our data.

The OH radical reactivity with I/SVOCs is the driving force for the formation of O_3 and many other

secondary pollutants (Dunmore et al., 2015). The rate coefficients k_{OH} of the gas-phase reactions

of OH radicals with these I/SVOCs have been estimated from Episuite (EPI, 2017) and are shown

17

in Table S8. Figure 4 shows the gas-phase concentrations and primary OH reactivity of alkanes (n+i), monocyclic alkanes, bicyclic alkanes and monocyclic aromatics at the roadside site MR and roof site RU. Alkanes (n+i) were the most abundant class in the gas phase (31% at MR and 44% in RU) followed by monocyclic alkanes (29% in MR and 24% in RU), monocyclic aromatics (23% in MR and 21% in RU) and bicyclic alkanes (16% in MR and 10% in RU). Cyclic alkanes react faster with OH radicals than alkanes (n+i) and monocyclic aromatics with the same carbon number, shown as higher rate coefficients k_{OH} in Table S8. Monocyclic and bicyclic alkanes are the species making the overwhelming contribution to the primary OH reactivity at MR (60%) and RU (51%) in this study. As expected, primary OH reactivity of the sum of the I/SVOC groups at roadside site MR was the greatest among the four sampling sites, followed by the urban background site EL and then the two roof sites. Whalley et al. (2016) measured the total OH reactivity at an urban background site in central London during a summer campaign. For the organic and inorganic classes they studied, NO_x and the carbonyl class of VOCs made the dominant contribution to the average OH reactivity in the ambient atmosphere (18.1 s^{-1}). The hydroxyl radical reactivity with the organic classes identified in this study only accounted for a very minor fraction of the magnitude of the total OH reactivity that Whalley et al. (2016) reported.

SOA is typically generated only from the oxidation of gaseous reactive organic compounds above C_7 as the vapour pressures of the oxidation products must be sufficiently low to enable the gas phase products to partition to the particle phase (Odum et al., 1997). Long-chain alkanes can play an important role in the formation of SOA as they are the main components of the unresolved complex mixture (UCM) in the fuel associated exhaust (Schauer et al., 1999;2002; Robinson et al.,2007). SOA created from alkanes with shorter chains includes the first and higher generation oxidation products, while SOA oxidised from the alkanes with very long chains is mainly from the first-generation products (Lim and Ziemann, 2005; Pye and Pouliot, 2012; Jordan et al., 2008). The

potential SOA formation generated by the oxidation of gas-phase SOA precursors were estimated

by the following equation (Chan et al., 2009),

$$\Delta\ M_{SOA,i} = [HCi] \times (1 - e^{-k_{OH,i}[OH]\Delta t}) \times Y_i$$

Where [HCi] is the measured concentrations of gas-phase SOA precursor i (ng m^{-3}); $k_{OH,i}$ is the rate

coefficients of the reactions of OH radicals with SOA precursor i (cm^3 molecule $^{-1}$ s^{-1}); [OH] is the

concentration of OH radicals (molecule cm^{-3}); Δt is the OH radical exposure time (s); and Y_i is the

SOA yield of the SOA precursor, i.

The potential SOA formation contributed by I/SVOC groups were estimated based on the

corresponding SOA yields (Table S9-S10) (Presto et al., 2010; Ng et al., 2007)The SOA yields

applied in this study were measured in chamber studies under urban-like conditions with an organic

aerosol mass C_{OA} of 7 µg m^{-3} which is the average organic matter concentration at MR and RU.

According to the UK NO$_x$ emission interactive map from the National Atmospheric Emissions

Inventory (NAEI) (https://naei.beis.gov.uk/emissionsapp/), the area within the London Orbital

Motorway M25 can be regarded as the high NO$_x$ emission area while the area outside of the M25 is

a low NO$_x$ emission area. With a distance of 20-30 km between the MR-RU-WM sampling area to

the M25, and a minimum wind speed of 1.5 m s^{-1} during the sampling period, there was assumed to

be around 6 h of SOA formation under the high-NO$_x$ regime. Hence, the SOA yields under high

NO$_x$ conditions were applied to estimate the SOA formation in the first 6 h and SOA yields under

low NO$_x$ conditions for SOA formation at 12 h and 36 h. SOA yields for n-alkanes from C$_{12}$ to C$_{17}$

under high-NO$_x$ conditions were derived from Presto et al. (2010) while for n-alkane C$_{12}$ under low-

NO$_x$ conditions were derived from Loza et al. (Loza et al., 2014). SOA yields for heavier n-alkanes,

branched alkanes and cyclic alkanes were estimated based on SOA yields of low-molecular weight

n-alkanes and the method developed by Pye and Pouliot (2012). Yields for monocyclic aromatics

19

derived from Ng et al. (2007) and Henze et al. (2008). The estimation processes for SOA yields and potential SOA formation are shown in Supplementary Information S3.

The predicted SOA formed by the photooxidation of the four main gas-phase chemical classes based upon concentrations measured at the roadside site MR at 3 h, 12 h and 36 h are shown in Figure 5. Two scenarios have been modelled which reflect the extreme cases but avoid the need to model the particle/vapour partitioning of semi-volatile compounds, for which insufficient data were available. Three of the panels in Figure 5 show results for oxidation of vapour only after 3 h, 12 h and 36 h respectively. The fourth panel shows the maximum potential SOA formation after 36 h if all particle-associated material had entered the vapour phase and been available for oxidation. The particle associated I/SVOCs will progressively evaporate and be oxidised with atmospheric dilution caused by the lack of equilibrium between the gas and the particle phase, creating substantial amounts of low-volatility gas-phase compounds (Robinson et al., 2007). Primary particle associated I/SVOCs may potentially contribute a considerable amount of SOA formed from C_{20}-C_{27} semi-volatile hydrocarbons (Figure 5). The SOA formation from the sum of gas phase and particle phase I/SVOCs at 36 h was estimated to present the maximum potential SOA formation and the realistic SOA formation likely lies between this and the SOA formed by gas phase compounds only. In the first 6 h, SOA yields reported in the high NO_x studies may not represent the highest possible yields as they were measured after 50-85% of alkanes have oxidised (Loza et al., 2014). Although monocyclic aromatics (C_{13} -C_{19}) accounted for a substantial fraction (over 20%) of the gas-phase emissions in this study, these compounds contribute only a small fraction (around 5%) of the SOA formed in the first 3 h of photooxidation due to their relatively low SOA yield and slow oxidation rate. This is consistent with the estimated SOA formation from diesel exhaust by Chan et al. (2009), who reported light aromatics ($\leq C_9$) contributed a much smaller fraction of SOA formation than their fraction in the total emission.

Alkane classes were the largest contributors to SOA formation in this study, and SOA yields of a given carbon number followed the order cyclic> linear>branched alkanes under high NO_x conditions (Loza et al., 2014). Although alkanes (n+i) were the most abundant class in the primary gas-phase emission, monocyclic alkanes contributed the greatest fraction of SOA formation (39%) at 3 h due to their substantial primary emission and more significant SOA yields. Bicyclic alkanes contributed 26% of the SOA formation, followed by n-alkanes (20%) and branched alkanes (10%) at 3 h at MR.

At 12 h and 36 h, the time is assumed to be sufficiently long to allow for 95-100% of the hydrocarbon to react with OH radicals if the chemical reaction during night-time and deposition of gas-phase hydrocarbons are ignored (Chan et al., 2009). After such a long time, hydrocarbons in ambient air are supposed to be transported from the emission source to more remote regions, where the NO_x level is lower (Henze et al., 2008; Chan et al., 2009). Studies suggest that SOA yields of alkane classes under low NO_x conditions follow the order: cyclic> linear ~branched alkanes (Loza et al., 2014). Gas phase cyclic alkanes still make the overwhelming contribution (54%-55%) to the SOA formation at 12-36h. Gas phase monocyclic aromatics made a greater contribution to SOA formation (9%-11%) at 12-36h compared with their contribution in the first 3h due to higher SOA yields under low NO_x conditions (Ng et al., 2007; Loza et al., 2014; Henze et al., 2008). At 36h, primary particle-phase branched alkanes (33%) made the greatest contribution to SOA formation, followed by monocyclic alkanes (26%) and bicyclic alkanes (22%), n-alkanes (18%) and monocyclic aromatics (3%) (Figure 5).

Figure 6 shows the changes of SOA formation with time from the oxidation of the semi-volatile hydrocarbon concentrations measured at RU. SOA formation from the RU gas-phase shows a steady increase with time under high NO_x conditions in the first 6 h, and then a more significant increase after 6 h due to higher SOA yields under low NO_x conditions. Yin et al. (2015) reported an

overall SOA of 2.95 µg m^{-3} at a London background site during winter, of which 55% of SOA is biogenic in origin and 45% of SOA is anthropogenic. The maximum SOA formation at 36 hours based upon the RU data amounts (both gas and particle phase) is around 0.4 µg m^{-3}, which is only accounted for 30% of the SOA formed by anthropogenic precursors reported by Yin et al., (2015). Zhao et al. (2014) predicted that gas-phase I/SVOCs contribute over four times more SOA in Los Angeles than the estimate here for London as a result of much higher I/SVOC concentrations measured in Los Angeles. The estimated SOA production is subject to considerable uncertainties. It takes no account of precursor dry and wet deposition processes (Knote et al., 2015), is dependent upon NO$_x$ concentrations with only yields for "high" and "low" NO$_x$ available, and yield from chamber experiments are influenced by chamber wall effects which are very difficult to correct for.

4.   CONCLUSION

This study has investigated the behaviour of I/SVOC groups collected in the FASTER London Campaign 2017. The consistency between the concentrations of low n-alkanes measured by the DEFRA network with those observed in this study gives confidence in the data and illustrates the importance of taking account of compounds of higher molecular weight. The CPI values of n-alkanes and the correlation analysis between measured compound groups with traffic indicators are consistent with traffic as a major contributor to I/SVOC at all four sites, while other sources make a minor contribution to the I/SVOC concentrations, especially for the heavier compounds (above C$_{25}$). More specifically, measured alkanes (acyclic and cyclic) and aromatic compounds at MR are mainly attributable to diesel-powered vehicles while a major proportion of the low molecular weight compounds is attributable to the gasoline-powered vehicles. One potential shortcoming of this study is that I/SVOC data are daily averages, but traffic volume typically has a strong diurnal cycle.

The partitioning of n-alkanes between the gas phase and the particle phase was examined in this study, showing shallower slopes (m_r) around -0.5 for the regression between Log Kp and Log(VPt). Many reasons have been discussed to explain the deviation of slopes m_r from the theoretical value of -1. This seems to be commonly observed for alkanes and in our data seems likely to result, at least in part, due to disequilibrium or to absorptive partitioning. Alkanes (n+i), cyclic alkanes and aromatics are important classes of I/SVOCs which react with OH radical leading to the formation of the secondary organic aerosol (SOA). Roadside MR had the fastest reactions followed by the rooftop sites WM and RU, due to their lower concentrations. Cyclic alkanes contribute overwhelmingly to the OH reactivity estimated in this study due to their relatively high rate coefficients k_{OH}. Cyclic alkanes also made the greatest contribution to the SOA formation due to their significant SOA yields and substantial primary emissions. Monocyclic aromatics contributed to only a small fraction of the SOA formation as a result of low SOA yields and slow oxidation rates although they accounted for a more substantial percentage of gas-phase emissions. At 36h, primary particle associated I/SVOCs were included to estimate the maximum potential SOA formation as they may evaporate and be oxidised at large downwind distances. The I/SVOCs measured in current study made a relatively small contribution to overall OH reactivity and SOA in London.

DATA ACCESSIBILITY

Data supporting this publication are openly available from the UBIRA eData repository at https://doi.org/10.25500/edata.bham.00000335

ACKNOWLEDGEMENTS

SUPPORTING INFORMATION

Supporting Information provides further details of air sampling sites and dates, grouped compound

concentrations, partitioning calculations, and calculations of OH reactivity and SOA yields.

CONFLICT OF INTERESTS

The authors declare no competing financial interest.

REFERENCE

Alam, M. S., Nikolova, I., Singh, A., Mackenzie, A. R. and Harrison, R. M. 2019. Experimental Vapour Pressures of Eight n-Alkanes (C_{17}, C_{18}, C_{20}, C_{22}, C_{24}, C_{26}, C_{28} and C_{31}) at Ambient Temperatures. Atmospheric Environment, 213, 739-74.

Alam, M. S., Zeraati-Rezaei, S., Liang, Z., Stark, C., Xu, H., Mackenzie, A. R. and Harrison, R. M. 2018. Mapping and quantifying isomer sets of hydrocarbons ($\geqslant C_{12}$) in diesel exhaust, lubricating oil and diesel fuel samples using GC$\times$GC-ToF-MS. Atmospheric Measurement Techniques, 11, 3047-3058.

Alam, M. S., Zeraati-Rezaei, S., Stark, C. P., Liang, Z., Xu, H. and Harrison, R. M. 2016a. The characterisation of diesel exhaust particles–composition, size distribution and partitioning. Faraday discussions, 189, 69-84.

Alam, M. S., Stark, C. and Harrison, R. M. 2016b. Using variable ionization energy time-of-flight mass spectrometry with comprehensive GCxGC to identify isomeric species. Analytical Chemistry, 88, 4211-4220.

Alves, C. A. 2008. Characterisation of solvent extractable organic constituents in atmospheric particulate matter: an overview. Anais da Academia Brasileira de Ciências, 80, 21-82.

Alves, C. A., Oliveira, C., Martins, N., Mirante, F., Caseiro, A., Pio, C., Matos, M., Silva, H. F., Oliveira, C. and Camões, F. 2016. Road tunnel, roadside, and urban background measurements of aliphatic compounds in size-segregated particulate matter. Atmospheric Research, 168, 139-148.

Andreou, G. and Rapsomanikis, S. 2009. Origins of n-alkanes, carbonyl compounds and molecular biomarkers in atmospheric fine and coarse particles of Athens, Greece. Science of the Total Environment, 407, 5750-5760.

Arp, H. P. H., Schwarzenbach, R. P. and Goss, K.-U. 2008. Ambient gas/particle partitioning. 2: The influence of particle source and temperature on sorption to dry terrestrial aerosols. Environmental Science & Technology, 42, 5951-5957.

Barley, M. and McFiggans, G. 2010. The critical assessment of vapour pressure estimation methods for use in modelling the formation of atmospheric organic aerosol. Atmospheric Chemistry and Physics, 10, 749-767.

Bi, X., Sheng, G., Peng, P. A., Chen, Y., Zhang, Z. and Fu, J. 2003. Distribution of particulate-and vapor-phase n-alkanes and polycyclic aromatic hydrocarbons in urban atmosphere of Guangzhou, China. Atmospheric Environment, 37, 289-298.

Bidleman, T. F., Billings, W. N. and Foreman, W. T. 1986. Vapor-particle partitioning of semivolatile organic compounds: estimates from field collections. Environmental Science & Technology, 20, 1038-1043.

Callén, M., De La Cruz, M., López, J., Murillo, R., Navarro, M. and Mastral, A. 2008. Some inferences on the mechanism of atmospheric gas/particle partitioning of polycyclic aromatic hydrocarbons (PAH) at Zaragoza (Spain). Chemosphere, 73, 1357-1365.

Chan, A. W. H., Kautzman, K., Chhabra, P., Surratt, J., Chan, M., Crounse, J., Kürten, A., Wennberg, P., Flagan, R. and Seinfeld, J. 2009. Secondary organic aerosol formation from photooxidation of naphthalene and alkylnaphthalenes: implications for oxidation of intermediate volatility organic compounds (IVOCs). Atmospheric Chemistry and Physics, 9, 3049-3060.

Chan, A. W. H., Isaacman, G., Wilson, K. R., Worton, D. R., Ruehl, C. R., Nah, T., Gentner, D. R., Dallmann, T. R., Kirchstetter, T. W., Harley, R. A., Gilman, J. B., Kuster, W. C., De Gouw, J. A., Offenberg, J. H., Kleindienst, T. E., Lin, Y. H., Rubitschun, C. L., Surratt, J. D., Hayes, P. L., Jimenez, J. L. and Goldstein, A. H. 2013. Detailed chemical characterization of unresolved complex mixtures in atmospheric organics: Insights into emission sources, atmospheric processing, and secondary organic aerosol formation. Journal of Geophysical Research: Atmospheres, 118, 6783-6796.

Charron, A., Polo-Rehn, L., Besombes, J.-L., Golly, B., Buisson, C., Chanut, H., Marchand, N., Guillaud, G. and Jaffrezo, J.-L. 2019. Identification and quantification of particulate tracers of exhaust and non-exhaust vehicle emissions. Atmospheric Chemistry & Physics, 19, 5187-5207.

Cincinelli, A., Bubba, M. D., Martellini, T., Gambaro, A. and Lepri, L. 2007. Gas-particle concentration and distribution of n-alkanes and polycyclic aromatic hydrocarbons in the atmosphere of Prato (Italy). Chemosphere, 68, 472-478.

Compernolle, S., Ceulemans, K. and Müller, J.-F. 2011. Evaporation: a new vapour pressure estimation methodfor organic molecules including non-additivity and intramolecular interactions. Atmospheric Chemistry and Physics, 11, 9431-9450.

Cross, E. S., Sappok, A. G., Wong, V. W., Kroll, J. H. 2015. Load-dependent emission factors and chemical characteristics of IVOCs from a medium-duty diesel engine. Environmental Science & Technology, 49, 13483-13491.

Drozd, G. T., Zhao, Y., Saliba, G., Frodin, B., Maddox, C., Oliver Chang, M. C., Maldonado, H., Sardar, S., Weber, R. J., Robinson, A. L. and Goldstein, A. H. 2019. Detailed Speciation of Intermediate Volatility and Semivolatile Organic Compound Emissions from Gasoline Vehicles: Effects of Cold-Starts and Implications for Secondary Organic Aerosol Formation. Environmental Science & Technology, 53, 1706-1714.

Dunmore, R., Hopkins, J., Lidster, R., Lee, J., Evans, M., Rickard, A., Lewis, A. and Hamilton, J. 2015. Diesel-related hydrocarbons can dominate gas phase reactive carbon in megacities. Atmospheric Chemistry and Physics, 15, 9983-9996.

El Haddad, I., Marchand, N., Dron, J., Temime-Roussel, B., Quivet, E., Wortham, H., Jaffrezo, J. L., Baduel, C., Voisin, D. and Besombes, J. L. J. A. E. 2009. Comprehensive primary particulate organic characterization of vehicular exhaust emissions in France. Atmospheric Environment, 43, 6190-6198.

EPI 2017. EPI Suite™ - Estimation Program Interface v4.11 [Online]. Available: https://www.epa.gov/tsca-screening-tools/download-epi-suitetm-estimation-program-interface-v411 [Accessed 18 Jan 2019].

Fernández, P., Grimalt, J. O. and Vilanova, R. M. 2002. Atmospheric gas-particle partitioning of polycyclic aromatic hydrocarbons in high mountain regions of Europe. Environmental Science & Technology, 36, 1162-1168.

Filliger, P., Puybonnieux-Texier, V. and Schneider, J., 1999, June. Health costs due to road traffic-related air pollution. An impact assessment project of Austria, France and Switzerland. Prepared for the WHO Ministerial Conference for Environment and Health, Geneva: WHO,. Citeseer. http://citeseerx.ist.psu.edu/viewdoc/download?doi=10.1.1.525.3110&rep=rep1&type=pdf

Foreman, W. T. and Bidleman, T. F. 1990. Semivolatile organic compounds in the ambient air of Denver, Colorado. Atmospheric Environment. Part A. General Topics, 24, 2405-2416.

Fraser, M. P., Cass, G. R., Simoneit, B. R. and Rasmussen, R. 1997. Air quality model evaluation data for organics. 4. C2-C36 non-aromatic hydrocarbons. Environmental Science & Technology, 31, 2356-2367.

Gaga, E. O. and Ari, A. 2011. Gas–particle partitioning of polycyclic aromatic hydrocarbons (PAHs) in an urban traffic site in Eskisehir, Turkey. Atmospheric Research, 99, 207-216.

Goldstein, A. H. and Galbally, I. E. 2007. Known and Unexplored Organic Constituents in the Earth's Atmosphere. Environmental Science & Technology, 41, 1515-1521.

Grieshop, A. P., Miracolo, M. A., Donahue, N. M. and Robinson, A. L. 2009. Constraining the volatility distribution and gas-particle partitioning of combustion aerosols using isothermal dilution and thermodenuder measurements. Environmental Science & Technology, 43, 4750-4756.

Gupta, S., Gadi, R., Mandal, T. K. and Sharma, S. K. 2017. Seasonal variations and source profile of n-alkanes in particulate matter (PM_{10}) at a heavy traffic site, Delhi. Environmental Monitoring & Assessment, 189, 43.

Harrison, R. M., Beddows, D. C. and Dall'Osto, M. 2011. PMF analysis of wide-range particle size spectra collected on a major highway. Environmental Science & Technology, 45, 5522-5528.

Harrison, R. M., Jones, A. M., Beddows, D. C. S., Dall'osto, M. and Nikolova, I. 2016. Evaporation of traffic-generated nanoparticles during advection from source. Atmospheric Environment, 125, 1-7.

Harrison, R. M. and Beddows, D. C. 2017. Efficacy of recent emissions controls on road vehicles in Europe and implications for public health. Scientific Reports, 7, 1152.

Harrison, R. M., Beddows, D. C. S., Alam, M. S., Singh, A., Brean, J., Xu, R., Kotthaus, S. and Grimmond, S. 2019. Interpretation of particle number size distributions measured across an urban area during the FASTER campaign. Atmospheric Chemistry and Physics, 19, 39-55.

He, L.-Y., Hu, M., Zhang, Y.-H., Huang, X.-F. and Yao, T.-T. 2008. Fine particle emissions from on-road vehicles in the Zhujiang Tunnel, China. Environmental Science & Technology, 42, 4461-4466.

Henze, D., Seinfeld, J., Ng, N., Kroll, J., Fu, T.-M., Jacob, D. J., Heald, C. J. A. C. and Heald, C. L. 2008. Global modeling of secondary organic aerosol formation from aromatic hydrocarbons: high-vs. low-yield pathways. Atmospheric Chemistry and Physics, 8, 2405-2420.

Isaacman, G., Wilson, K. R., Chan, A. W., Worton, D. R., Kimmel, J. R., Nah, T., Hohaus, T., Gonin, M., Kroll, J. H. and Worsnop, D. R. 2012. Improved resolution of hydrocarbon structures and constitutional isomers in complex mixtures using gas chromatography-vacuum ultraviolet-mass spectrometry. Analytical chemistry, 84, 2335-2342.

Jathar, S. H., Miracolo, M. A., Presto, A. A., Donahue, N. M., Adams, P. J. and Robinson, A. L. 2012. Modeling the formation and properties of traditional and non-traditional secondary organic aerosol: problem formulation and application to aircraft exhaust. Atmospheric Chemistry and Physics, 12, 9025-9040.

Jordan, C., Ziemann, P., Griffin, R., Lim, Y., Atkinson, R. & Arey, J. 2008. Modeling SOA formation from OH reactions with C8–C17 n-alkanes. Atmospheric Environment, 42, 8015-8026.

Karanasiou, A., Sitaras, I., Siskos, P. and Eleftheriadis, K. 2007. Size distribution and sources of trace metals and n-alkanes in the Athens urban aerosol during summer. Atmospheric Environment, 41, 2368-2381.

Kawashima, H., Minami, S., Hanai, Y. and Fushimi, A. 2006. Volatile organic compound emission factors from roadside measurements. Atmospheric Environment, 40, 2301-2312.

Khare, P. and Gentner, D. R. 2018. Considering the future of anthropogenic gas-phase organic compound emissions and the increasing influence of non-combustion sources on urban air quality. Atmospheric Chemistry and Physics,18, 5391-5413.

Knote, C., Hodzic, A. and Jimenes, J.L. 2015. The effect of dry and wet deposition of condensable vapours on secondary organic aerosols concentrations over the continental US. Atmospheric Chemistry & Physics, 15, 1-18.

Kwon, E. E. and Castaldi, M. J. 2012. Mechanistic understanding of polycyclic aromatic hydrocarbons (PAHs) from the thermal degradation of tires under various oxygen concentration atmospheres. Environmental science & technology 46, 12921-12926.

Leskinen, A. P., Jokiniemi, J. K. and Lehtinen, K. E. J. 2007. Transformation of diesel engine exhaust in an environmental chamber. Atmospheric Environment, 41, 8865-8873.

Lewis, A. C., Carslaw, N., Marriott, P. J., Kinghorn, R. M., Morrison, P., Lee, A. L., Bartle, K. D. and Pilling, M. J. 2000. A larger pool of ozone-forming carbon compounds in urban atmospheres. Nature, 405, 778-781.

Lim, Y. B. and Ziemann, P. J. 2005. Products and mechanism of secondary organic aerosol formation from reactions of n-alkanes with OH radicals in the presence of NO_x. Environmental Science & Technology, 39, 9229-9236.

Lim, Y. B. and Ziemann, P. J. 2009. Effects of molecular structure on aerosol yields from OH radical-initiated reactions of linear, branched, and cyclic alkanes in the presence of NO_x. Environmental Science & Technology, 43, 2328-2334.

Loza, C. L., Craven, J. S., Yee, L. D., Coggon, M. M., Schwantes, R. H., Shiraiwa, M., Zhang, X., Schilling, K. A., Ng, N. L., Canagaratna, M. R., Ziemann, P. J., Flagan, R. C. and Seinfeld, J. H. 2014. Secondary organic aerosol yields of 12-carbon alkanes. Atmospheric Chemistry and Physics, 14, 1423-1439.

Lu, Q., Zhao, Y., Robinson, A. L. 2018. Comprehensive organic emission profiles for gasoline, diesel, and gas-turbine engines including intermediate and semi-volatile organic compound emissions. Atmospheric Chemistry & Physics, 18, 17637-17654.

Lyu, R., Alam, M. S., Stark, C., Xu, R., Shi, Z., Feng, Y. and Harrison, R. M. 2019. Aliphatic carbonyl compounds (C_8–C_{26}) in wintertime atmospheric aerosol in London, UK. Atmospheric Chemistry and Physics, 19, 2233-2246.

Mader, B. T. and Pankow, J. F. 2001. Gas/solid partitioning of semivolatile organic compounds (SOCs) to air filters. 2. Partitioning of polychlorinated dibenzodioxins, polychlorinated dibenzofurans, and polycyclic aromatic hydrocarbons to quartz fiber filters. Atmospheric Environment, 35, 1217-1223.

Mandalakis, M., Tsapakis, M., Tsoga, A. and Stephanou, E. G. 2002. Gas–particle concentrations and distribution of aliphatic hydrocarbons, PAHs, PCBs and PCDD/Fs in the atmosphere of Athens (Greece). Atmospheric Environment, 36, 4023-4035.

May, A. A., Presto, A. A., Hennigan, C. J., Nguyen, N. T., Gordon, T. D. and Robinson, A. L. 2013. Gas-particle partitioning of primary organic aerosol emissions: (2) Diesel vehicles. Environmental Science & Technology, 47, 8288-8296.

Mazurek, M. and Simoneit, B. 1984. Characterization of biogenic and petroleum-derived organic matter in aerosols over remote, rural and urban areas. Identification and Analysis of Organic Pollutants in Air, 22, 353.

McDonald, B. C., De Gouw, J. A., Gilman, J. B., Jathar, S. H., Akherati, A., Cappa, C. D., Jimenez, J. L., Lee-Taylor, J., Hayes, P. L. and Mckeen, S. A. 2018. Volatile chemical products emerging as largest petrochemical source of urban organic emissions. Science. 359, 760-764.

Met. Office 2006. MIDAS: UK Hourly Weather Observation Data. NCAS British Atmospheric Data Centre [Online]. Available: http://catalogue.ceda.ac.uk/uuid/916ac4bbc46f7685ae9a5e10451bae7c [Accessed 21 March 2019].

Mirante, F., Alves, C., Pio, C., Pindado, O., Perez, R., Revuelta, M. A. and Artiñano, B. 2013. Organic composition of size segregated atmospheric particulate matter, during summer and winter sampling campaigns at representative sites in Madrid, Spain. Atmospheric Research, 132-133, 345-361.

NAEI, 2019. National Atmospheric Emissions Inventory, http://naei.beis.gov.uk [Accessed 21 March 2019].

Ng, N., Kroll, J., Chan, A., Chhabra, P., Flagan, R. and Seinfeld, J. 2007. Secondary organic aerosol formation from m-xylene, toluene, and benzene. Atmospheric Chemistry and Physics, 7, 3909-3922.

Nikolova, I., Mackenzie, A. R., Cai, X., Alam, M. S. and Harrison, R. M. 2016. Modelling component evaporation and composition change of traffic-induced ultrafine particles during travel from street canyon to urban background. Faraday Discussions, 189, 529-546.

O'Meara, S., Booth, A. M., Barley, M. H., Topping, D. and McFiggans, G. 2014. An assessment of vapour pressure estimation methods. Physical Chemistry Chemical Physics, 16, 19453-19469.

Odum, J. R., Jungkamp, T., Griffin, R. J., Forstner, H., Flagan, R. C. and Seinfeld, J. H. 1997. Aromatics, reformulated gasoline, and atmospheric organic aerosol formation. Environmental Science & Technology, 31, 1890-1897.

Omar, N. Y. M. J., Abas, M. R. B., Rahman, N. A., Tahir, N. M., Rushdi, A. I. and Simoneit, B. R. T. 2007. Levels and distributions of organic source tracers in air and roadside dust particles of Kuala Lumpur, Malaysia. Environmental Geology, 52, 1485-1500.

Pankow, J. F. 1994. An absorption model of gas/particle partitioning of organic compounds in the atmosphere. Atmospheric Environment, 28, 185-188.

Pankow, J. F. and Bidleman, T. F. 1992. Interdependence of the slopes and intercepts from log-log correlations of measured gas-particle paritioning and vapor pressure - I. theory and analysis of available data. Atmospheric Environment. Part A. General Topics, 26, 1071-1080.

Pant, P., Shukla, A., Kohl, S. D., Chow, J. C., Watson, J. G. and Harrison, R. M. 2015. Characterization of ambient PM2. 5 at a pollution hotspot in New Delhi, India and inference of sources. Atmospheric Environment, 109, 178-189.

Presto, A. A., Miracolo, M. A., Donahue, N. M. and Robinson, A. L. 2010. Secondary organic aerosol formation from high-NO$_x$ photo-oxidation of low volatility precursors: n-alkanes. Environmental Science & Technology, 44, 2029-2034.

Presto, A. A., Hennigan, C. J., Nguyen, N. T. and Robinson, A. L. 2012. Determination of volatility distributions of primary organic aerosol emissions from internal combustion engines using thermal desorption gas chromatography mass spectrometry. Aerosol Science Technology, 46, 1129-1139.

Pye, H. O. and Seinfeld, J. H. 2010. A global perspective on aerosol from low-volatility organic compounds. Atmospheric Chemistry and Physics, 10, 4377-4401.

Pye, H. O. and Pouliot, G. A. 2012. Modelling the role of alkanes, polycyclic aromatic hydrocarbons, and their oligomers in secondary organic aerosol formation. Environmental Science & Technology, 46, 6041-6047.

Robinson, A. L., Donahue, N. M., Shrivastava, M. K., Weitkamp, E. A., Sage, A. M., Grieshop, A. P., Lane, T. E., Pierce, J. R. and Pandis, S. N. 2007. Rethinking organic aerosols: Semivolatile emissions and photochemical aging. Science, 315, 1259-1262.

Rogge, W. F., Hildemann, L. M., Mazurek, M. A., Cass, G. R. and Simoneit, B. R. 1993. Sources of fine organic aerosol. 3. Road dust, tire debris, and organometallic brake lining dust: roads as sources and sinks. Environmental Science & Technology, 27, 1892-1904.

Sakurai, H., Tobias, H. J., Park, K., Zarling, D., Docherty, K. S., Kittelson, D. B., Mcmurry, P. H. and Ziemann, P. J. 2003. On-line measurements of diesel nanoparticle composition and volatility. Atmospheric Environment, 37, 1199-1210.

Sangiorgi, G., Ferrero, L., Perrone, M., Papa, E. and Bolzacchini, E. 2014. Semivolatile PAH and n-alkane gas/particle partitioning using the dual model: up-to-date coefficients and comparison with experimental data. Environmental Science and Pollution Research, 21, 10163-10173.

Schauer, J. J., Kleeman, M. J., Cass, G. R. and Simoneit, B. R. 1999. Measurement of emissions from air pollution sources. 2. C1 through C30 organic compounds from medium duty diesel trucks. Environmental Science & Technology, 33, 1578-1587.

Schauer, J. J., Kleeman, M. J., Cass, G. R. and Simoneit, B. R. 2002. Measurement of emissions from air pollution sources. 5. C_1-C_{32} organic compounds from gasoline-powered motor vehicles. Environmental Science & Technology, 36, 1169-1180.

Simoneit, B. R. T. 1999a. A Review of Biomarker Compounds as Source Indicators and Tracers for Air Pollution. Environmental Science & Pollution Resesearch, 6,159-169

Simoneit, B. R., Kobayashi, M., Mochida, M., Kawamura, K., Lee, M., Lim, H. J., Turpin, B. J. and Komazaki, Y. 2004. Composition and major sources of organic compounds of aerosol particulate matter sampled during the ACE‐Asia campaign. Journal of Geophysical Research: Atmospheres, 109, D19S10.

Terzi, E. and Samara, C. 2004. Gas-particle partitioning of polycyclic aromatic hydrocarbons in urban, adjacent coastal, and continental background sites of western Greece. Environmental Science & Technology, 38, 4973-4978.

Tkacik, D. S., Presto, A. A., Donahue, N. M. and Robinson, A. L. 2012. Secondary organic aerosol formation from intermediate-volatility organic compounds: cyclic, linear, and branched alkanes. Environmental Science & Technology, 46, 8773-8781.

Topping, D., Barley, M., Bane, M., Higham, N. J., Aumont, B., Dingle, N. and McFiggans, G. 2016. UManSysProp v1. 0: an online and open-source facility for molecular property prediction and atmospheric aerosol calculations. Geoscientific Model Development, 9, 899-914.

UManSysProp. 2016. Available: http://umansysprop.seaes.manchester.ac.uk/tool/vapour_pressure [Accessed 18 Jan 2019].

Wehner, B., Birmili, W., Gnauk, T. and Wiedensohler, A. 2002. Particle number size distributions in a street canyon and their transformation into the urban-air background: measurements and a simple model study. Atmospheric Environment, 36, 2215-2223.

Weitkamp, E. A., Sage, A. M., Pierce, J. R., Donahue, N. M. and Robinson, A. L. 2007. Organic aerosol formation from photochemical oxidation of diesel exhaust in a smog chamber. Environmental Science & Technology, 41, 6969-6975.

Whalley, L., Stone, D., Bandy, B., Dunmore, R., Hamilton, J.F., Hopkins, J., Lee, J.D., Lewis, A.C. and Heard, D.E. 2016. Atmospheric OH reactivity in central London: observations, model predictions and estimates of in situ ozone production. Atmospheric Chemistry and Physics, 16, 2109-2122.

Yamasaki, H., Kuwata, K. and Miyamoto, H. 1982. Effects of ambient temperature on aspects of airborne polycyclic aromatic hydrocarbons. Environmental Science & Technology, 16, 189-194.

Worton, D. R., Isaacman, G., Gentner, D. R., Dallmann, T. R., Chan, A. W., Ruehl, C., Kirchstetter, T. W., Wilson, K. R., Harley, R. A. and Goldstein, A. H. 2014. Lubricating oil dominates primary organic aerosol emissions from motor vehicles. Environmental Science & Technology, 48, 3698-3706.

Xu, R., Alam, M. S., Stark, C. and Harrison, R. M. 2019. Composition and emission factors of traffic- emitted intermediate volatility and semi-volatile hydrocarbons (C_{10}-C_{36}) at a street canyon and urban background sites in central London, UK. Submitted to Atmospheric Environment.

31

Yin, J., Cumberland, S. A., Harrison, R. M., Allan, J., Young, D. E., Williams, P. I. and Coe, H. 2015. Receptor modelling of fine particles in southern England using CMB including comparison with AMS-PMF factors. Atmospheric Chemistry & Physics, 15, 2139-2158.

Zhao, Y., Hennigan, C. J., May, A. A., Tkacik, D. S., De Gouw, J. A., Gilman, J. B., Kuster, W. C., Borbon, A. and Robinson, A. L. 2014. Intermediate-volatility organic compounds: a large source of secondary organic aerosol. Environmental Science & Technology, 48, 13743-13750.

Zhao, Y., Nguyen, N. T., Presto, A. A., Hennigan, C. J., May, A. A. and Robinson, A. L. 2016. Intermediate volatility organic compound emissions from on-road gasoline vehicles and small off-road gasoline engines. Environmental Science & Technology, 50, 4554-4563.

TABLE LEGEND:

Table 1. Average gas and particulate phase concentrations of n-alkanes and CPI of London samples.

Table 2. Summary of concentrations of n-alkanes (ng/m^3) in the air samples. Gas and particle indicate the gas phase and particle phases.

FIGURE LEGENDS:

Figure 1. Average concentrations of n-alkanes from the DEFRA network (C_2-C_8) and GC×GC-MS (C_{13}-C_{31} in the gas phase and particle phase) at MR (top panel) from March to April 2017 and at EL (bottom panel) from February to March 2017.

Figure 2. Pearson correlation coefficient R between I/SVOCs and traffic indicators at MR, WM and RU.

Figure 3. Log Kp vs log (Vpt) plots for n-alkanes (C_{13}-C_{29}) in all samples at MR and RU.

Figure 4. The mass concentrations of I/SVOCs and primary hydrocarbon OH reactivity (h^{-1}) grouped by carbon number at MR and RU.

Figure 5. The potential SOA formation in 3h, 12h, 36h calculated from MR I/SVOCs.

Figure 6. Potential SOA generated from the gas phase in the first 3h, 6h, 12h, 36h (first y-axis) and generated from the particle phase and total (gas+particle phase) in 36h (secondary y-axis) based upon concentrations measured at RU.
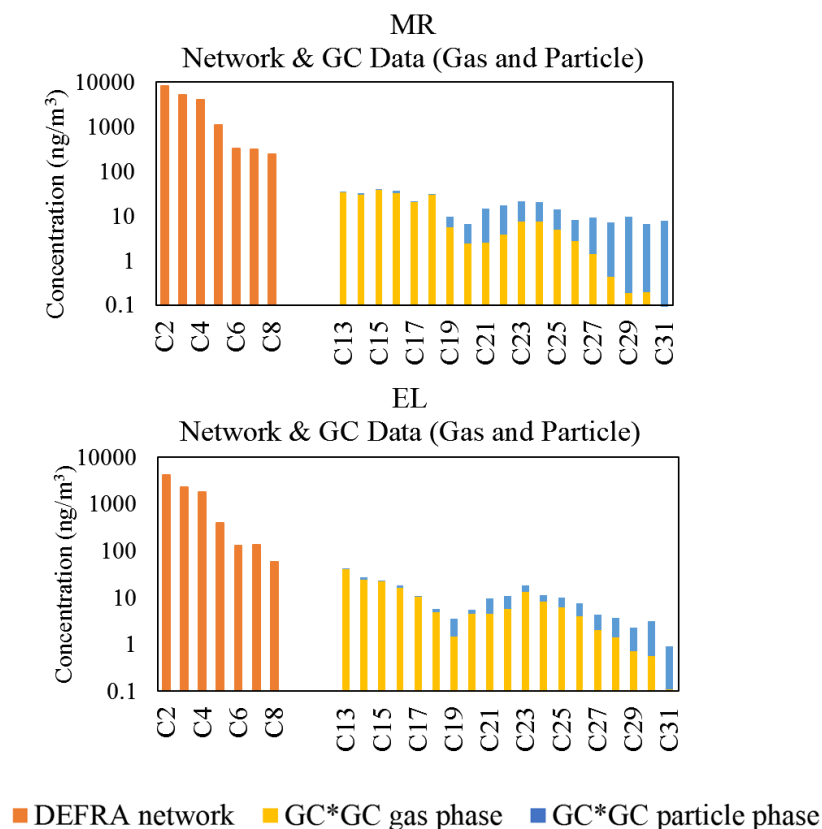
33

Table 1. Average gas and particulate phase concentrations of n-alkanes and CPI of London samples.

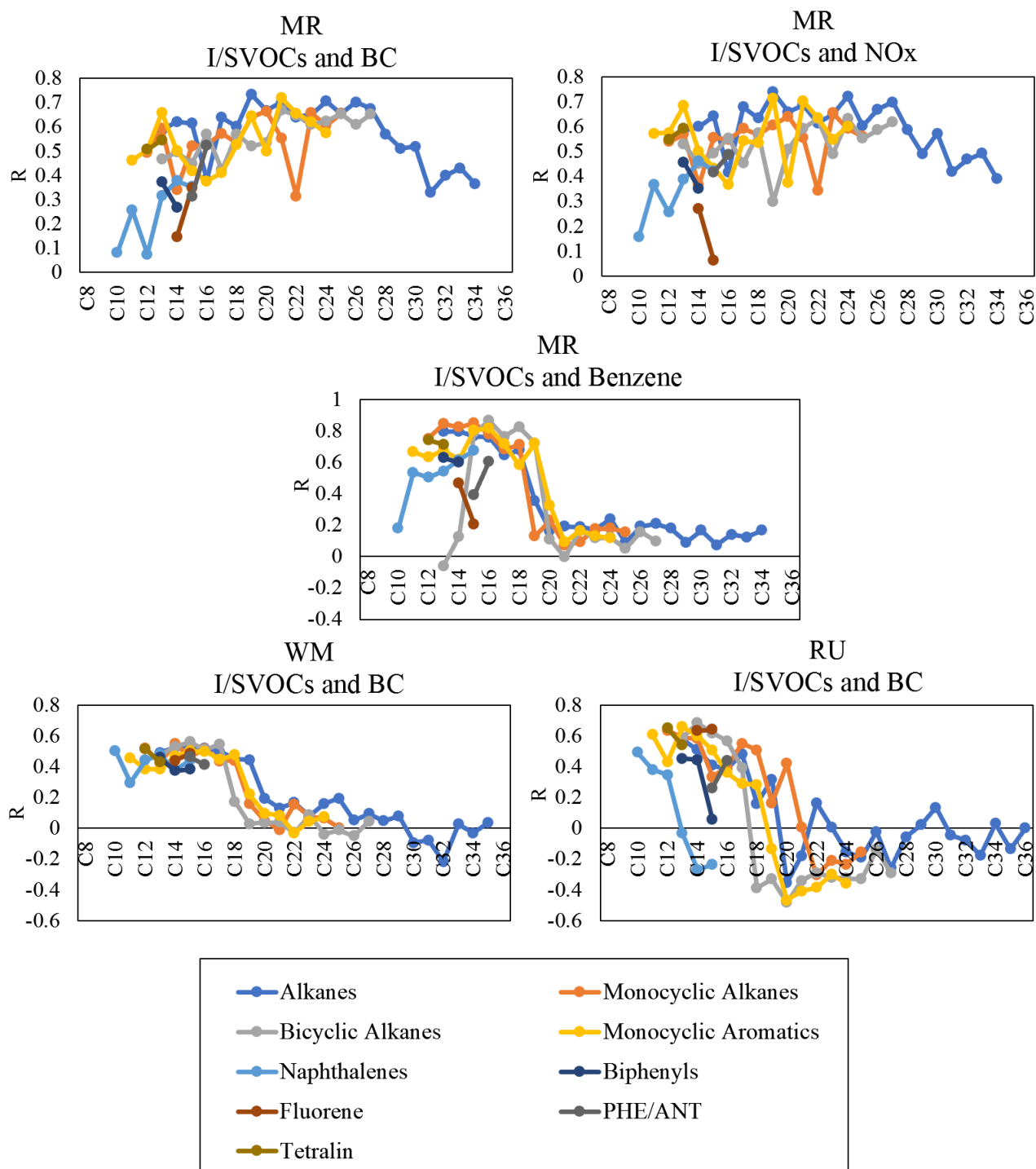| n-alkanes	Gas Phase (ng/m^3)				Particulate Phase (ng/m^3)			
Carbon No	WM	RU	MR	EL	WM	RU	MR	EL
C13	19.77	13.91	33.94	40.13	0.90	0.79	1.42	1.23
C14	17.02	10.45	30.31	24.55	1.96	1.59	2.17	2.57
C15	17.03	10.21	37.98	22.15	0.70	0.90	1.55	0.84
C16	16.69	10.35	32.28	16.20	1.13	0.75	3.78	1.84
C17	10.46	6.29	20.72	10.48	0.17	0.31	0.25	0.49
C18	13.78	7.99	29.58	4.84	0.63	0.98	1.37	0.93
C19	3.56	1.64	5.50	1.49	0.92	0.95	3.91	2.05
C20	1.64	0.53	2.42	4.42	0.95	0.97	4.19	1.15
C21	1.36	0.40	2.51	4.57	5.43	2.32	11.87	5.12
C22	1.04	0.43	3.78	5.70	6.85	2.43	13.58	5.04
C23	4.68	2.95	7.48	13.23	5.05	4.16	14.25	4.78
C24	4.01	2.23	7.34	8.28	3.00	2.42	13.22	2.87
C25	2.24	1.33	4.87	6.16	2.78	2.58	8.95	3.98
C26	1.42	0.70	2.68	3.94	2.23	1.83	5.46	3.66
C27	0.71	0.25	1.37	1.99	1.37	1.26	7.75	2.28
C28	0.43	0.16	0.43	1.43	1.10	1.14	6.63	2.19
C29	0.27	0.07	0.18	0.72	2.16	1.58	9.41	1.60
C30	0.23	0.06	0.19	0.56	0.89	1.06	6.53	2.62
C31					0.65	0.83	7.61	0.80
C32					0.63	0.80	8.65	0.06
C33					0.64	0.90	7.75	0.09
C34					0.23	0.67	0.66	0.02
C35					0.35	0.73		0.12
C36					0.13	0.45		0.07
$\sum NA$	116.35	69.96	223.57	170.85	40.85	32.41	141.0	46.40
CPI*	1.07	1.13	1.05	1.44	1.08	1.17	1.13	1.02
CPI (C$_{13}$-C$_{26}$)	1.06	1.12	1.04	1.45	0.95	1.10	0.96	1.02
CPI (above C$_{25}$)	1.55	1.80	1.95	1.50	1.59	1.39	1.48	1.03

* CPI (C$_{13}$-C$_{30}$) for the gas phase and CPI (C$_{13}$-C$_{36}$) for the particle phase.

Table 2. Summary of concentrations of n-alkanes (ng/m^3) in the air samples. Gas and particle indicate the gas phase and particle phases.
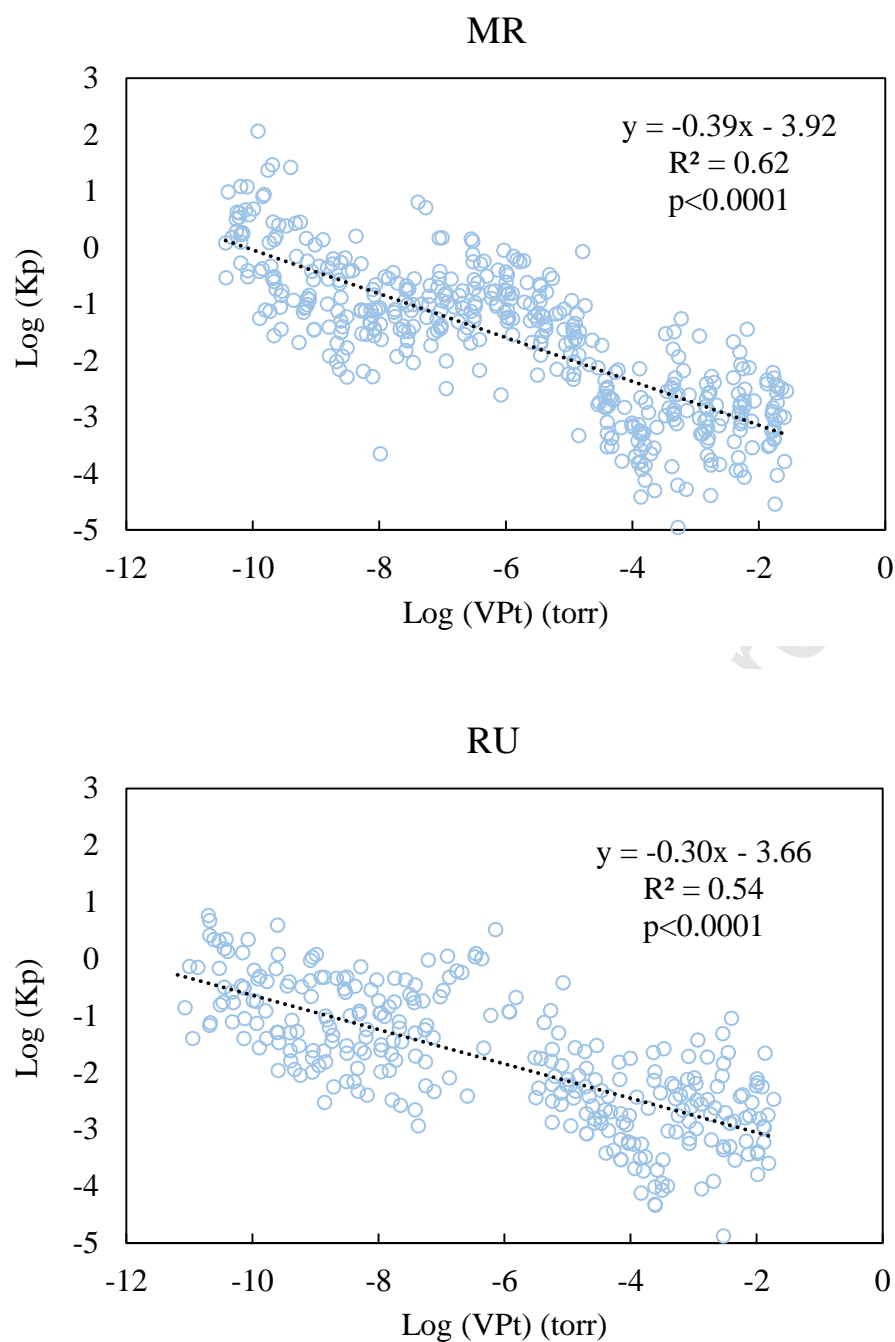
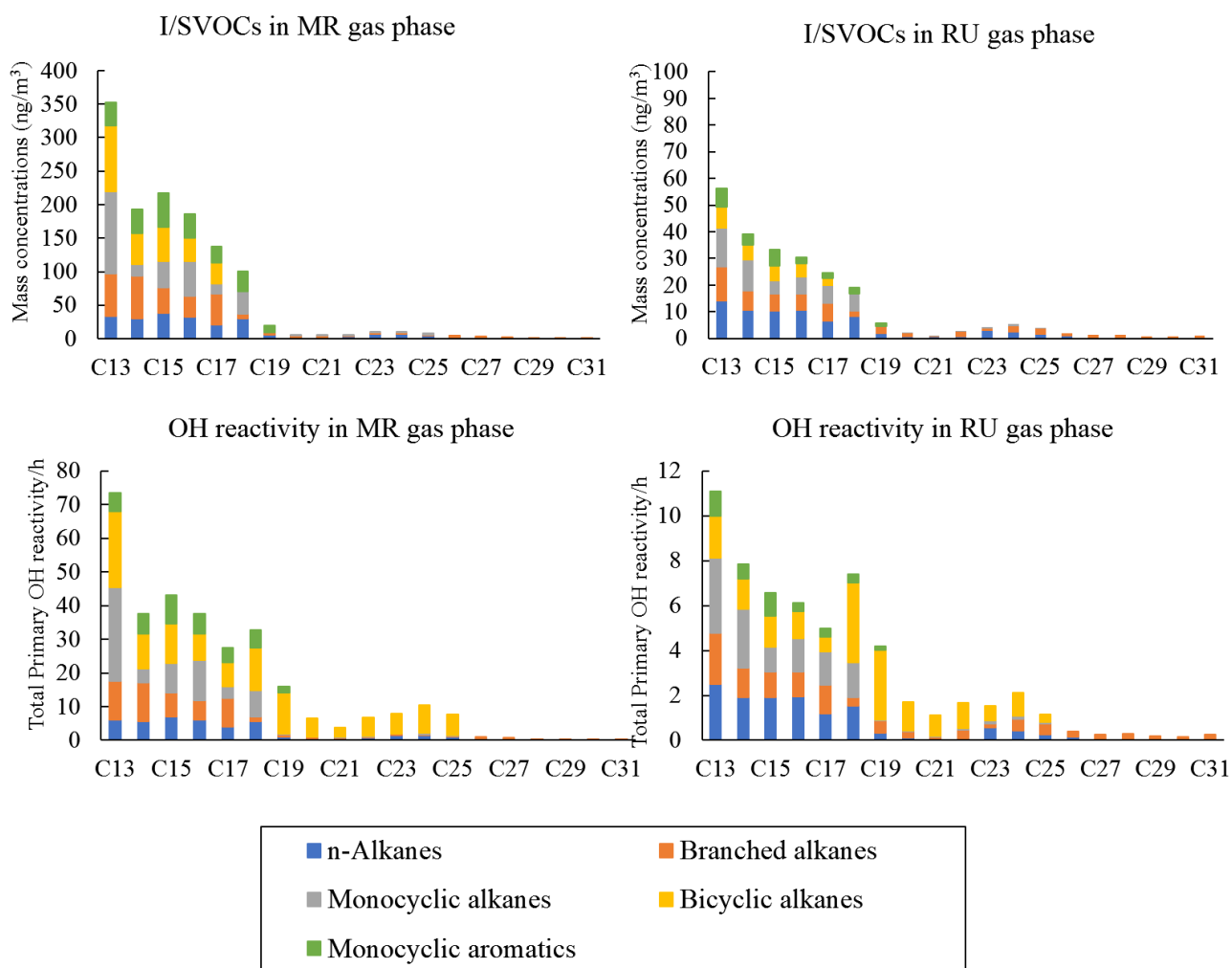| Carbon No	Prato Italy (Cincinelli et al., 2007)		Delhi India (Gupta et al., 2017)	Birmingham UK (Nikolova et al., 2016)		Athens Greece (Mandalakis et al., 2002)		Guangzhou, China (Bi et al., 2003)	Athens Greece (Karanasiou et al., 2007)
	Industry area Mar-Nov		Heavily trafficked site Jan-Feb	Busy traffic road (BROS) year 1999/2000		Urban background July		Urban area April	Heavy trafficked central avenue Jun-Jul
	Gas	Particle	Particle (PM_{10})	Gas	Particle	Gas	Particle	Gas and particle	Particle
C_{13}								0.51	
C_{14}			6			0.83		1.44	
C_{15}	3		5			1.83	0.10	2.14	
C_{16}	8	<1	4.8	6.42	0.65	3.89	0.15	8.25	
C_{17}	16	<1	4	9.32	0.85	4.00	0.09	23.73	
C_{18}	23	<1	5	9.36	0.82	5.07	0.10	62.00	87.2±110
C_{19}	30	<1	5	9.74	1.32	5.20	0.19	149.28	14.8±6.5
C_{20}	32.5	1	6	8.35	1.93	3.92	0.31	226.10	44.6±56.4
C_{21}	30.5	1	7.5	6.20	2.63	5.05	0.52	216.23	14.7±6.8
C_{22}	24.5	2.5	7.8	3.97	3.25	3.86	0.76	168.07	42.2±46.9
C_{23}	18	4.8	12	2.32	2.73	3.97	1.41	117.97	29.8±21.9
C_{24}	13	8	17.5	1.59	3.34	2.70	1.50	90.41	57.5±55.3
C_{25}	7	14	19	1.20	4.46	2.17	2.71	78.03	55.0±46.7
C_{26}	<1	17.5	12	1.00	2.37	1.44	2.35	54.43	65.6±57.8
C_{27}	2	22.5	15	1.28	3.61	1.25	5.28	42.97	43.3±36.4
C_{28}	1.5	14	11	1.03	1.89	1.13	2.19	32.26	34.0±27.5
C_{29}	1.8	18	9	1.24	4.89	1.21	8.25	38.37	25.1±21.0
C_{30}	1.5	9	7.5	0.8	2.03	0.98	1.85	25.55	13.6±13.9
C_{31}	1.5	18	7.8	0.77	3.60	0.85	8.54	44.05	14.2±15.0
C_{32}	1	6	10	0.42	1.32	0.41	1.42	15.89	8.5±14.9
C_{33}	<1	6	9.5			0.52	1.23	23.79	10.2±15.8

35

Figure 1. Average concentrations of n-alkanes from the DEFRA network (C_2-C_8) and GC×GC-MS (C_{13}-C_{31} in the gas phase and particle phase) at MR (top panel) from March to April 2017 and at EL (bottom panel) from February to March 2017.
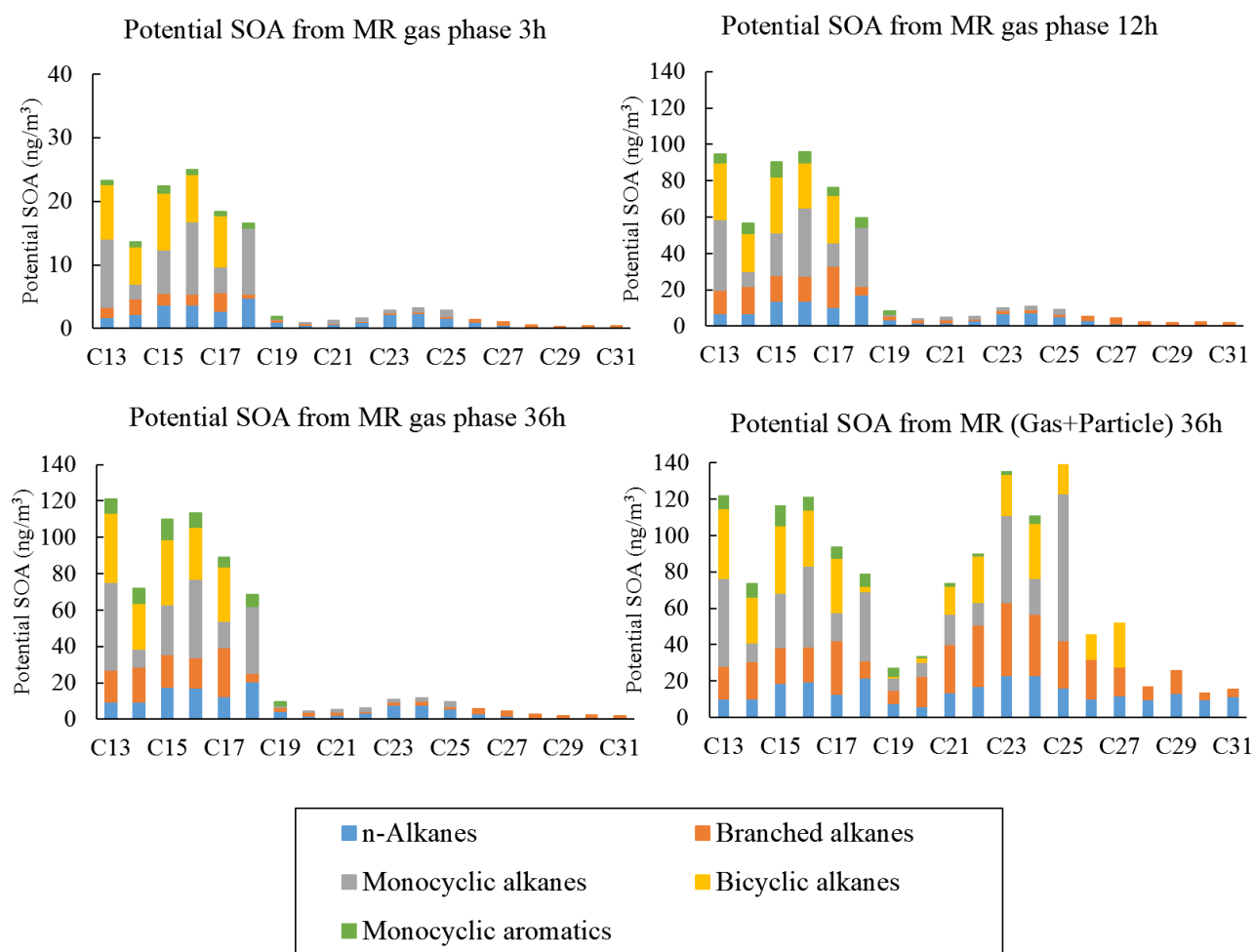
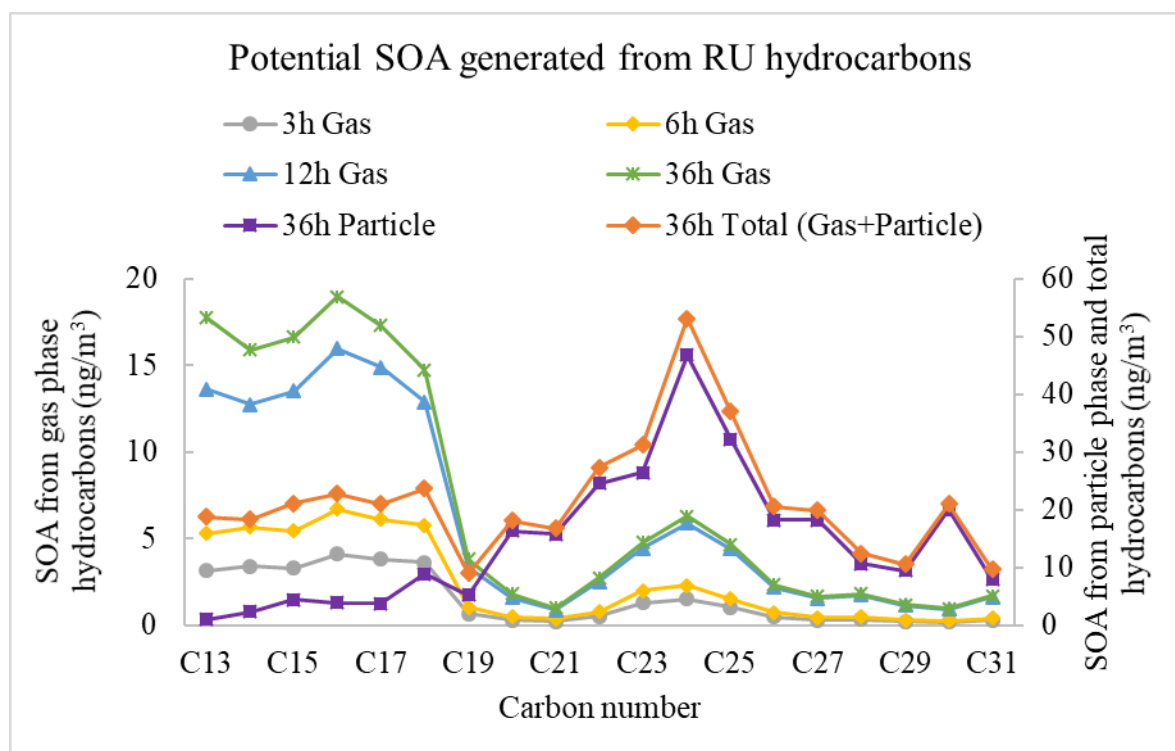**Figure 2.** Pearson correlation coefficient R between I/SVOCs and traffic indicators at MR, WM and RU.

MR

$$y = -0.39x - 3.92$$
$$R^2 = 0.62$$
$$p<0.0001$$

RU

$$y = -0.30x - 3.66$$
$$R^2 = 0.54$$
$$p<0.0001$$

Figure 3. Log Kp vs log (Vpt) plots for n-alkanes (C_{13}-C_{29}) in all samples at MR and RU.

38

Figure 4. The mass concentrations of I/SVOCs and primary hydrocarbon OH reactivity (h^{-1}) grouped by carbon number at MR and RU.

Figure 5. The potential SOA formation in the 3h, 12h, 36h calculated from MR I/SVOCs.

40

Figure 6. Potential SOA generated from the gas phase in the first 3h, 6h, 12h, 36h (first y-axis) and generated from the particle phase and total (gas+particle phase) in 36h (secondary y-axis) based upon concentrations measured at RU.

42

Conflict of interest

The authors have no actual or potential conflict of interest including any financial, personal or other relationships with other people or organizations within three years of beginning the submitted work that could inappropriately influence, or be perceived to influence, their work.

Behaviour of Traffic Emitted Semi-Volatile and Intermediate Volatility Organic Compounds Within the Urban Atmosphere

HIGHLIGHTS

- Measurements of particulate and vapour phase hydrocarbons made at sites in London

- Intermediate volatility and semi-volatile (C_{10}-C_{36}) compounds analysed

- Concentrations of alkanes (straight, branched and cyclic) and aromatics

- CPI, partitioning, OH reactivity and SOA formation potential evaluated

- Diesel emissions are dominant source